

Context-based vector fields for multi-object tracking in application to road traffic

Egor Sattarov, Sergio Alberto Rodriguez Florez, Alexander Gepperth, Roger Reynaud

▶ **To cite this version:**

Egor Sattarov, Sergio Alberto Rodriguez Florez, Alexander Gepperth, Roger Reynaud. Context-based vector fields for multi-object tracking in application to road traffic. IEEE International Conference On Intelligent Transportation Systems (ITSC), Oct 2014, Qingdao, China. pp.1179 - 1185, 10.1109/ITSC.2014.6957847 . hal-01098701v2

HAL Id: hal-01098701

https://inria.hal.science/hal-01098701v2

Submitted on 28 Dec 2014

HAL is a multi-disciplinary open access archive for the deposit and dissemination of scientific research documents, whether they are published or not. The documents may come from teaching and research institutions in France or abroad, or from public or private research centers.

L'archive ouverte pluridisciplinaire **HAL**, est destinée au dépôt et à la diffusion de documents scientifiques de niveau recherche, publiés ou non, émanant des établissements d'enseignement et de recherche français ou étrangers, des laboratoires publics ou privés.

Context-based vector fields for multi-object tracking in application to road traffic

Egor Sattarov[1,2,3], Sergio A. Rodríguez F.[1,2], Alexander Gepperth[3], Roger Reynaud[1,2]
[1]*Université Paris-Sud*, [2]*CNRS Institut d'Électronique Fondamentale UMR 8622*
[3]*Ecole Nationale Supérieure de Techniques Avancées, France*

***Abstract*—In this contribution, we propose to use road and lane information as contextual cues in order to increase the precision of multi-object object tracking. For tracking, we employ a Monte Carlo implementation of a Probability Hypothesis Density (PHD)-filter, whereas scene context (road and lane information) is taken from annotated street maps. The novel aspect of the presented work is the tightly coupling of context information and the particle filtering process. This is achieved by injecting a priori particles representing locally expected motions, which are in turn determined by the local road and the lane configuration.**

This approach is evaluated on objects (tracklets) from the public KITTI benchmark database. Our experimental findings demonstrate a considerable tracking precision increasing when including this kind of a priori knowledge. At the same time, the approach is able to determine objects whose movements differ from the locally expected motion, which is an important feature for safety applications.

***Keywords*—Multi-tracking, Probability Hypothesis Density Filter, Particle filter, Vector field, Intelligent vehicle, Road context**

I. Introduction

After more than 30 years of contributions on Multiple Target Tracking (MTT), this subject still remains open since, depending on the applications, it addresses complex problems such as management of multiple hypotheses, data association between multiple information sources, and real time constraints. In the context of Intelligent Vehicles (IV), MTT is a key perception process attempting to determine the (e.g. kinematic) state of observed objects. This information is not only important for active safety applications, such as Advanced Driver Assistance Systems (ADAS), but also for scene understanding in autonomous vehicles.

I-A. Related work

Classic MTT approaches are defined by a recursive framework where a set of detected objects is managed by means of temporal filtering such as Kalman or particle filters. Filtering can usually cope with detection errors and simple missed detections. Multiple Hypothesis Tracking (MHT, [14]), and Joint Probability Data Association Filtering (JPDAF, [1], [7], are part of well-known mechanisms improving the performance of tracking for complex object-to-track association cases in the presence of missed and false detections.

The PHD filter algorithm is efficient in terms of computational resources and propagates the first-order moments of multi-object statistics [10], [17], [12], [19], [18]. PHD is capable to filter clutter, missing observations along with noisy ones using the full Bayesian basis, just like MTT, but with linear complexity depending the number of tracked objects.

Recently, efficient particle implementations of PHD filtering have been proposed [18], [10], [12]. These approaches include the estimation of the number of observed tracks. To this end, particle clustering is necessary to identify tracks. However, such a procedure is non-trivial in urban scenarios where objects move in close proximity to each other. In our variant of the particle-based PHD-filter, we avoid the problems of clustering and cardinality estimation by initializing tracks with a fixed number of particles constantly attached to them. The method used by us is not claiming to perform superior multi-object tracking, however, it does facilitate the integration of contextual information, as particles are easy to affect by context information.

Temporal filtering contained in MTT frameworks exploits motion models and observed measurements for maximizing the probability of the observed motion. Interactive motion models take advantage of multiple expected high-level motion classes, such as lane changes or turns or stops at crossroads in application to IV contexts [6], [3]. Those models use online information about recent vehicle motions to predict their future positions. In our case, no motion model classes have been defined, but low-level primitives have been integrated in the form of expected velocity vector fields. Such vector fields are defined by road and lane context, which is in turn taken from maps using ego-localization information.

I-B. Contribution

Most of the state-of-the-art methods, which exploit context information, are strongly correlated to a particular detection method. For instance, road detection approaches [15], [2], [16], [5], are used to provide key information for driving assistance applications or to define regions of interest for object tracking [2], [11]. In contrast, this study is inspired by [9], [8], [13], [11] and aims to use extracted context (road) information to directly improve the quality of multi-object tracking. Our contribution in this article is a computational mechanism for integrating a priori knowledge

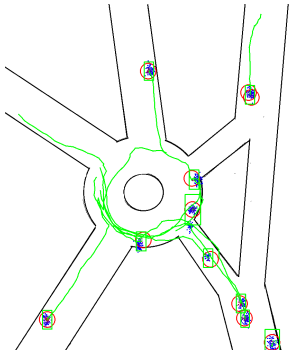


Figure 1: Example of a simulated multi-target tracking scene. Green rectangles are tracks, red circles are detections, dots are particles

derived from contextual road and lane information into a state-of-the-art multi-object tracking system. The benefits of this approach are evaluated in terms of track continuity and track overlapping.

II. Proposed methods

Our goal is to track vehicles, pedestrians and other possible objects in two-dimensional space (top-view) while taking scene context into account. Two use cases are considered: simulated scenarios on a featureless 2D map plane with hand-crafted velocity vector field as illustrated in Fig. 1, and a 2D East-North map space as shown in Fig. 2 taken from the KITTI-database, from which we obtain object information and GPS coordinates for the extraction of road and lane context via OpenStreetMap.

II-A. PHD-filter-based tracker

The PHD filter is represented by N^x dynamically changing tracks x_k, $k = \overline{1, N^x}$. Each track x contains N^p particles. Particle $\xi_{x_k,n}$, $n = \overline{1, N^p}$ contain a set of vectors $\{[c_i, d_i, v_i]^T\}$, $i = \overline{1, D}$, where D is dimension of the state space, c_i is the center coordinate, d_i is the detection scale and v_i is the speed. A weight $\omega_{x_k,n}$, $n = \overline{1, N^p}$ is assigned to each particle $\xi_{x_k,n}$, $n = \overline{1, N^p}$. The parameters of the PHD filter are: death probability P_d, birth probability P_b, false negative probability P_{fn} and a vector of resampling and association parameters σ_i, $i = \overline{1, D}$. The tracking process is composed of the following stages: prediction, association, observation, resampling, merging and correction.

1) Prediction : Tracks and theirs particles are propagated according to the motion model:

$$c_{i,t|t-1} = c_{i,t-1} + v_{i,t-1} \tag{1}$$
$$d_{i,t|t-1} = d_{i,t-1}, \quad i = \overline{1, D} \tag{2}$$
$$v_{i,t|t-1} = v_{i,t-1} \tag{3}$$

where t is a timestamp and $t-1$ is a previous timestamp.

2) Association : Input observations z_j, where $j = \overline{1, N^z}$ and N^z is a number of observations, are assigned to existing tracks x_k, $k = \overline{1, N^x}$. Tracks assigned to observations increase their associated probability by P_d:

$$P_{k,t} = \max(P_{k,t-1} + P_d, 1), \quad k = \overline{1, N^x} \tag{4}$$

Non-associated tracks update their probability by:

$$P_{k,t} = \max(P_{k,t-1} - P_d, 0) \tag{5}$$

Observations which are not associated create new tracks with a probability:

$$P_{k,t} = P_b \tag{6}$$

In case a new track is created, the weights of its particles are:

$$\omega_{x_k,n} = P_{k,t}/N^p, \quad n = \overline{1, N^p} \tag{7}$$

In detail, we proceed as follows:

– For all pairs $\{z_j, x_k\}$, $j = \overline{1, N^z}; k = \overline{1, N^x}$ the distance $G(x_{k,t}, z_{j,t})$ is calculated, where the distance function is a product of Gaussians:

$$\begin{aligned} G(x_{k,t}, z_{j,t}) = \mathcal{N}(c_{x_k,i} - c_{z_j,i}|0, K_c\sigma_i) \\ \times\mathcal{N}(d_{x_k,i} - d_{z_j,i}|0, K_d\sigma_i) \\ \times\mathcal{N}(v_{x_k,i} - v_{z_j,i}|0, K_v\sigma_i) \end{aligned} \tag{8}$$

where K_c, K_d, K_v are coefficients in the range $(0, 1]$, chosen empirically.

– Calculate an association threshold θ^a, as a distance:

$$\theta^a = G(x_{k,t}, \hat{x}_{k,t}) \tag{9}$$

where:

$$c_{\hat{x}_k,i} = c_{x_k,i} + K_c\sigma_i \tag{10}$$
$$d_{\hat{x}_k,i} = d_{x_k,i} + K_d\sigma_i \tag{11}$$
$$v_{\hat{x}_k,i} = v_{x_k,i} + K_v\sigma_i \tag{12}$$

– Find the nearest pair

$$(x, z) = \underset{x_k \in X, z_j \in Z}{\arg\max}\, G(x_k, z_j) \tag{13}$$

Associate these x and z, remove x from list of pairs to associate and repeat this step if:

$$G(x, z) > \theta^a \tag{14}$$

– Finally, a list of associated pairs $\{z_j, x_k\}$, a list of non-associated detections $\{z_j\}$ and a list of non-associated tracks $\{x_k\}$ are obtained.

3) Observation : For each new observation $z_{j,t}$, $j = 1, N^z$, and for each particle ξ_{x_k}, $x_k \in X$ a distance is calculated: $G(\xi_{x_k}, z_{j,t})$. The distances are normalized relative to observations:

$$\omega_{x_k,n} = \sum_j \frac{G(\xi_{x_k}, z_j)}{\sum_l G(\xi_{x_l}, z_j)} + \omega_{x_k,n} \times P_{fn} \tag{15}$$

The last term represents the "old" particle weights in order to stabilize fluctuations.

4) Resampling : Track x_k is deleted if

$$P_k < \theta^d \tag{16}$$

Where θ^d is an imposed parameter. Otherwise, its particles are resampled using random fluctuations:

$$c_{i,t} = c_{i,t|t-1} + \zeta_c(0, \hat{K}_c\sigma_i) \tag{17}$$

$$d_{i,t} = d_{i,t|t-1} + \zeta_d(0, \hat{K}_d\sigma_i) \tag{18}$$

$$v_{i,t} = v_{i,t|t-1} + \zeta_v(0, \hat{K}_v\sigma_i) \tag{19}$$

Here $\zeta_c, \zeta_d, \zeta_v$ are different white noises, and $\hat{K}_c, \hat{K}_d, \hat{K}_v$ are coefficients, chosen empirically.

The special multiplier $\hat{K}$ increases parameters $\hat{K}_c, \hat{K}_d, \hat{K}_v$ if track's probability is lower than one (this is done in order to make particles more dispersed when a track is "lost", making it easier to "pick up" the track later).

5) Merging: If two tracks x_{k1} and x_{k2} have a distance:

$$G(x_{k1}, x_{k2}) > \theta^m \tag{20}$$

they are supposed to belong to a single object, and the newer track is deleted. Here θ^m is a predefined merging threshold.

6) Correction: New track centers are calculated as the weighted mean of particles associated to that track:

$$x_{k,t} = \frac{1}{N^p} \sum_{n=1,N^p} \xi_{x_k,n,t} \tag{21}$$

The output of the algorithm is represented as a set of tracks.

II-B. Vector field implementation

The context information to implement in the tracking system is represented as a vector field, that is, a field of probable directions for each map location. If Π is the state space of tracking having dimension D, and a subspace $\mathbf{T} \subset \Pi$ is a space where vector fields are defined, then one point $\tau \in \mathbf{T}$ contains a set of N^τ vectors V in it. One vector $v \in V$ has components v_i, $i = \overline{1, D}$.

1) Orientation and norm influence: A track's coordinates c_i, $i = \overline{1, D}$ indicate a point of the tracking space $\pi \in \Pi$. At the resampling and association stages, when random fluctuations at point $\pi \in \mathbf{T}$ are needed, the vector field is applied. The $N \times (1 - C_{MF})$ first particles are resampled as in eqns.(17,18,19), and other particles are resampled according to vectors, defined in π in eqns.(22,23,24). Here C_{MF} is a coefficient of "model force". Particle resampling is performed as follows:

$$c_{i,t} = c_{i,t|t-1} + \zeta_c \tag{22}$$

$$d_{i,t} = d_{i,t|t-1} + \zeta_d \tag{23}$$

$$v_{i,t} = v_{\pi_j,i} + \zeta_v \tag{24}$$

where v_{π_j} is a vector defined at the point π, with components $v_{\pi_j,i}$, $i = \overline{1, D}$. All $N \times C_{MF}$ field-defined particles are divided between vectors v_{π_j}, $j = \overline{1, N^\pi}$ uniformly. Here N^π is a number of vectors defined in π.

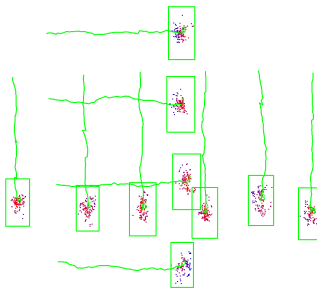


Figure 3: An example of a simulated scenario. The color of particles shows their weight and thus their current impact. The red particles have more weight than blue ones. Green rectangles indicate current tracks.

2) Direction-only influence: Another potential way to incorporate context consists in letting only the orientation of the vector field influence tracking. In this case, one can calculate new vector components as follows:

$$\hat{v}_{\pi_j,i} = \frac{v_{\pi_j,i} \times \left\|v_{t|t-1}\right\|}{\left\|v_{\pi_j}\right\|} \tag{25}$$

Here $\left\|v_{t|t-1}\right\|$ is the norm of the track's speed and $\left\|v_{\pi_j}\right\|$ is the norm of the vector field's speed at π_j. So, we fuse the field's orientation with the norm of the current track's speed. A visual representation of the vector field for the road map is illustrated in Fig. 2

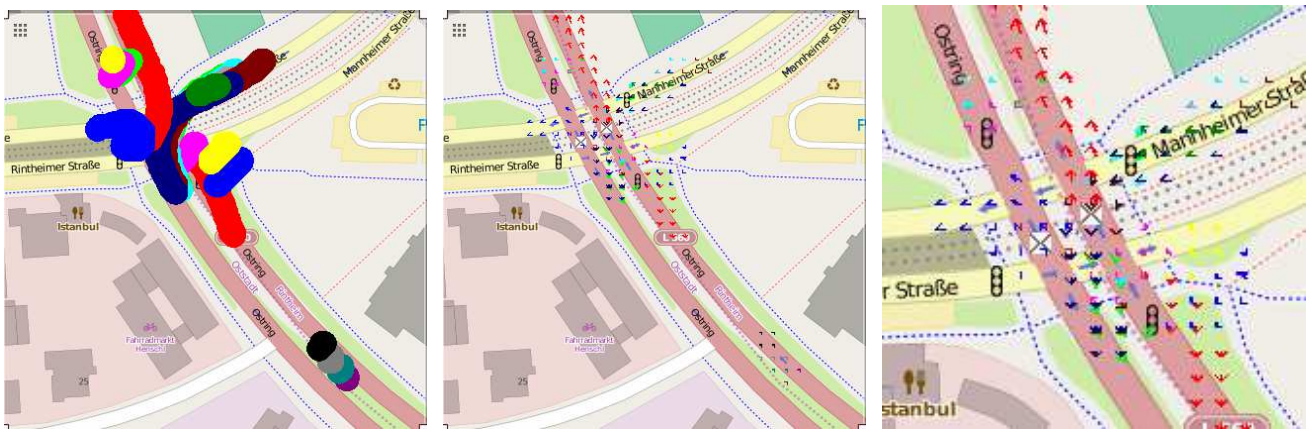
Especially the second point is important as it eliminates the need to use vector fields containing all possible speeds (vector lengths).

II-C. Vector field compatibility measurement

When the field of possible directions is imposed, it is clear that a moving object may not at all follow these directions. In such a case, it may be assumed that the object has atypical behavior and is therefore potentially dangerous. The detection of such objects is possible with the proposed framework. If the motion of a tracked object satisfies the condition (26) for at least one j, it can be classified as typical. The condition considers motion as being "typical" if field-sampled particles are closer to new detections than the mean of all particles. Fig. 3 shows a visual distribution of particles' weights.

$$\frac{\sum_{n \in \hat{N}^{\pi_j}} \omega_{x_k,n}}{\sum_{n \in \hat{N}^p} \omega_{x_k,n}} \times \frac{N^p}{C_{MF}/N^{\pi_j}} > 1 \tag{26}$$

Here, $\hat{N}$ and $\hat{N}^{\pi_j}$ are the sets of indexes for all particles of object and particles, resampled according to vector j of point π respectively.



(a) Map with areas covering by vector fields (b) Field's vector directions (c) Field's vector directions, zoom-in

Figure 2: Visual representation of vector fields on a OpenStreetMap (OSM) map

II-D. Evaluation method

Two major evaluation methods are used to quantify the accuracy of our approach: an overlap measure and a continuity measure. The first method measures the accuracy of a track's position with respect to associated real object position. The "continuity" measure computes the quality object-to-track associations. Track overlap is calculated as the mean of all association overlaps (i.e. overlap between track and real object):

$$Overlap = \frac{1}{N^{assoc}} \sum_{(k,i)} \max\left(\frac{S(x_k \cap y_i)}{S(x_k)}, \frac{S(x_k \cap y_i)}{S(y_i)}\right) \quad (27)$$

where N^{assoc} is a number of associations in XZ^{assoc} and S$(\cdot)$ is an area occupied by detection. The overlap value is always $\in [0, 1]$, where 1 represents the ideal case of full overlap.

The "continuity" measure is calculated according to the formula:

$$Continuity = \frac{1}{N^Y} \sum_{y_i \in Y} \max_k \frac{1}{N^{y_i}} \sum_t \delta_{k,i}(t) \quad (28)$$

where N^Y is a number of ground-truth objects, N^{y_i} is the number of appearances of the object y_i during the whole tracking scenario, $\delta_{k,i}(t) = 1$ if $(k, i) \in XZ^{assoc}(t)$ and $\delta_{k,i}(t) = 0$ otherwise. The continuity measure thus describes the mean of the longest associations. It varies in $(0, 1]$, where 1 is the ideal case of constant associations.

III. Experiments

The approach was tested on simulated data and on the public KITTI benchmark dataset[4] using annotated tracklets as ground-truth. The common schema to evaluate results requires four sets of data:

1. The set of labeled rectangles representing tracks constructed by our algorithms: X.
2. The set of labeled rectangles representing real objects Y, or ground-truth.
3. The set of labeled rectangles representing noisy objects Z. It is obtained from ground-truth by artificially introducing missed (false negative) detections, and by corrupting retained detections by noise. Noise is modeled as an additional Gaussian fluctuation applied to positions and sizes (c_i, d_i), $i = \overline{1, D}$ of all ground-truth objects. Each noisy detection $z \in Z$ has a ground-truth pair $y \in Y$.
4. The set of pairs of labels representing associations between noisy detections and tracks XZ^{assoc}

As the particle implementation of PHD-filtering contains a pseudo-random process, small variations can occur over trials. To precisely calculate the evaluation measures, the results were calculated as the mean and the variation of both measures across 15 trials.

III-A. Simulation

The first simulation scenario represents a scene of size 1000×1000 pixels and of 110 frames, with 10 objects moving simultaneously: four from left to right, six from up to down as shown in Fig. 4a. This scenario is chosen since it contains many pairwise intersections, in order to observe the algorithm's capability to resolve collisions. All of objects have sizes of 30×60 pixels.

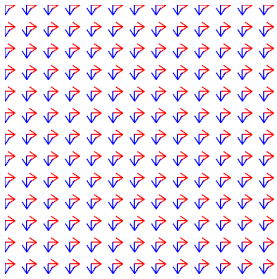
Noise parameters were set as follows:

1. $\sigma_d = 10$ - the variance of white noise applied to particle dimensions
2. $\sigma_c = 30$ - the variance of white noise applied to particle centers
3. False negative rate $P_{fn} = 0.1$
4. False positive rate $P_{fp} = 0.2$

PHD imposed parameters are:

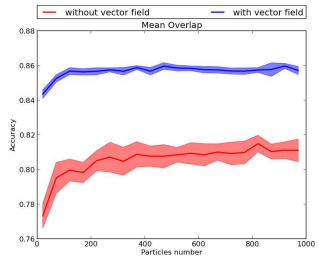


(a) (b)

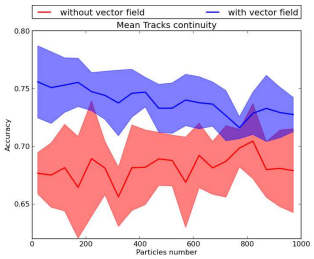


(c)

Figure 4: Visual representation of the vector field (c) and simulated scenarios (a,b). Green rectangles and traces are tracks and their previous positions



(a) Overlap



(b) Continuity

Figure 5: Accuracy for simulated data when only vector directions are used, plotted as a function of total particle number. Solid lines are mean values, semi-transparent borders represent their variances

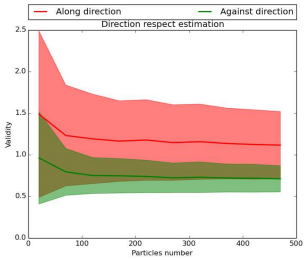


Figure 6: Direction compatibility measurements for simulated data. The values are calculated according to eqn. (26). For values bigger than 1.0, we assume movement along the field, and against the field otherwise.

1. $P_b = 0.7$
2. $P_d = 0.1$
3. $P_{fn} = 0.1$

The vector field map was created manually and covers all of the scene uniformly with two directions present: ”right” and ”down” as shown at Fig. 4c.

Estimations of overlap and continuity are shown at Fig. 5. A larger improvement of evaluation measures is observed for the overlap, i.e., position estimation, and a lower one for time continuity. However both measures are consistently improved by the introduction of the vector field.

Errors of associations can happen mostly in case of intersections. If two tracks meet at one point, they lose parts of their particle information which can help to resolve the collision because vector fields are identical and come from the same point position. But, on the other hand, if two differently oriented tracks meet in one point, the vector field at this point helps them to go through it faster. These two reasons balance themselves and so the impact of the vector field is low.

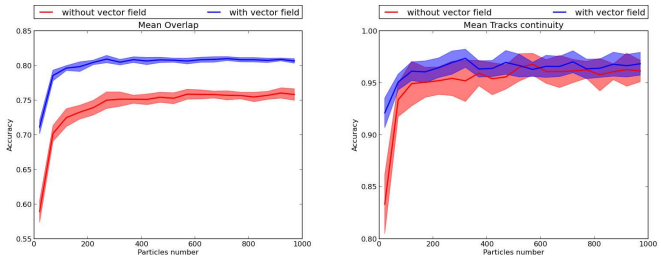
The overlap errors arise from imprecise positions of associations. When the position noise is Gaussian, the trajectories of tracks try to oscillate. When applying vector fields, this stabilizes positions and thus brings them closer to their mean, i.e. to real state.

For the same simulated scenario, vector field compatibility measures were calculated according to Sec. II-C. We measured their mean and standard deviation, both for ”compatible” and ”incompatible” tracks, with the expectation that the compatibility measure allows to distinguish those cases. The compatible tracks were evaluated in the scenario described above, the incompatible ones in a scenario with an inverted vector field but which was otherwise identical. The results are shown in Fig. 6. The difference in mean values is evident, but noise deviations are considerable.

The second simulation scenario represents a scene of size 1000×1000 pixels and of 200 frames, with 8 objects simultaneously: four compatible and four incompatible as it is shown at Fig. 4b. All of objects have sizes of 15×15 pixels. Noise parameters were set as follows: $\sigma_d = 10$, $\sigma_c = 20$, $P_{fn} = 0.2$, $P_{fp} = 0.125$. PHD imposed parameters are: $P_b = 0.7$, $P_d = 0.1$, $P_{fn} = 0.5$. This scenario is used to test auto-determined model force mechanism.

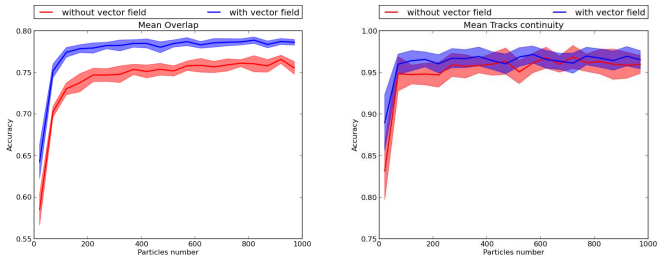
III-B. Real data

The tracking space is a 2D East-North plane limited of size 165×167 meters shown in Fig. 2. The duration of tracking is 12 seconds with a frequency of 8.9 fps. A number of 19 targets takes part in this urban traffic scenario. Since objects like cars, buses, pedestrians and cyclists are present without class distinction, detections of pedestrians can be mixed with detections of cars and other objects.



(a) Overlap (b) Continuity

Figure 7: Accuracy for real data for both vector directions and norms used in dependency of used particles number



(a) Overlap (b) Continuity

Figure 8: Accuracy for real data for only vector directions used in dependency of used particles number

Noise parameters were set to: $\sigma_d = 0$, $\sigma_c = 0.5$ meters, $P_{fn} = 0.1$, $P_{fp} = 0$. PHD imposed parameters are: $P_b = 0.7$, $P_d = 0.1$, $P_{fn} = 0.1$.

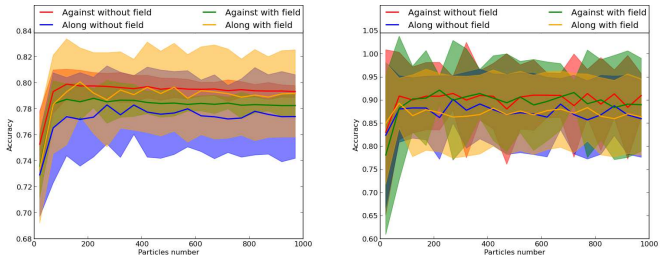
The vector field map was created manually based on OpenStreetMap and KITTI Velodyne and GPS-data and covers all tracklets' possible occupation areas with directions collateral to expected target motions in those areas. The map of directions is displayed in Figs. 2b,2c

Estimations of overlap and continuity in cases of full information are shown at Figs. 7,8. As in case of simulated data, the overlap shows a greater performance difference as a consequence of the vector field. The variance of performance is smaller because of less noise occurring in the real scenario.

From the comparison of the two cases: direction+norm vs direction only, and from the comparison of margins between baseline and vector field-affected performance, it is possible to draw the conclusion that in real road traffic the value of speed is a helpful information, but that one can still obtain significant gains in tracking quality when using only directions.

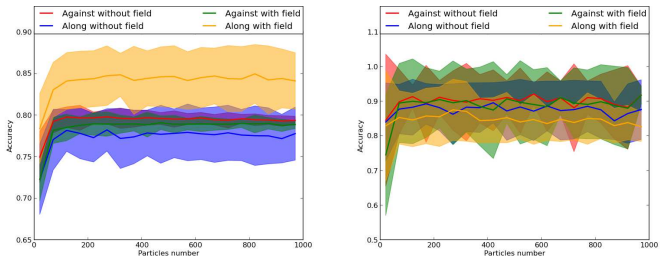
III-C. Auto-determined model force

The second simulated scenario mentioned in Sec. III-A was created to compare the impact on tracking precision



(a) Overlap (b) Continuity

Figure 9: Comparison of accuracy for tracks moving along and against vector fields without and with them using fixed model force coefficient



(a) Overlap (b) Continuity

Figure 10: Comparison of accuracy for tracks moving along and against vector fields without and with them using a variable model force coefficient

in the case of movements along vector fields to the case of movements against it. As expected, the results obtained during this experiment show a decreased tracking performance when tracks are incompatible with the context fields. In Fig. 9, four lines are shown where blue and red are the respective baselines for compatible and incompatible tracks without the influence of vector fields. Yellow and green curves represent compatible and incompatible tracks assisted by context with a fixed model force coefficient, $C_{MF} = 0.05$. As illustrated, the overlap observed for incompatible tracks is the almost the same as the improvement for compatible ones. Track continuity seems not be influenced in both cases.

Hereafter, we addressed the question of how to keep the advantages of contextual information while reducing the undesirable effects on incompatible tracks. To this end, a dynamic estimation of the model force coefficient, C_{MF}, is proposed. If the track is considered as compatible with respect to the vector field, see eqn. (26), C_{MF} is increased by 0.01 or decreased otherwise. For all tracks,C_{MF} varies from 0.01 to 0.5. The results are shown in Fig. 10

The overlap improvement for compatible tracks clearly outweighs the slight performance decrease observed for incompatible ones. However, track continuity decreases par-

ticularly for compatible tracks. This result can be explained in ambiguous tracking situations (e.g. two tracks intersecting) where contextual information can induce object-to-track association errors. Simulated scenarios contain objects intersecting at the same location with different speed directions. This use case is however not encountered under real conditions.

IV. Discussion

We presented a principled method to introduce prior knowledge into tracking, in this case information about expected object speeds obtained from scene context. We showed, both in a simulated and a real scenario from the KITTI database, that the quality of tracking (measured by standard measures) is significantly improved, leading to a more robust trajectory and motion estimation by a tracking algorithm. Although different tracking algorithms will implement this differently, the proposed vector field approach can be transferred to all particle-based tracking models and thus has a rather wide range of applicability.

Please note that, in this article, we have not addressed the subject of object *detection*: object information, or ground-truth, is available in both the simulated and the real scenario that we consider, and we corrupt it artificially by noise in order to show the benefits of our approach. Particularly when detections are obtained, as it is envisioned, from a real object detection system, our approach will be beneficial because the motion priors may conceivably lead to a better position estimation than it would be possible from noisy detections alone.

The Gaussian noise applied to simulate the detection jitter is not very realistic, and results may be slightly worse for a less convenient noise model. However it is simple to implement, and gives a good guess of performance under noise.

V. Conclusion

In this paper, we presented a proof-of-concept of a novel method for multiple target tracking for Intelligent Vehicles. This method uses road information in order to provide contextual cues which lead to an increased precision in multi-object tracking, suing a PHD filter approach in it's particle implementation. The public KITTI benchmark database was used to verify the impact on tracking precision, providing that such kind of a priori knowledge is considerably helpful when there is no single a priori direction but a distribution over them. The automatic detection of objects that violate the imposed priors was studied with favorable results, promising applicability in safety applications. Several points are still open, in particular how to correctly encode vector fields (with or without speed component). A subset of Gaussian-distributed particles with modified speed vectors, as used in this article, is a possibility, but other distributions, or a more complex particle state including potential high-level behaviors, are conceivable as well. Immediate future work will include a more representative testing using a marge set of urban traffic scenarios, provide more findings regarding the robustness of the proposed methodology.

References

[1] Habtemariam B., Tharmarasa R., Thayaparan T., and Mallick M. A multiple-detection joint probabilistic data association filter. 7:461 – 471, 2013.

[2] Roland Chapuis, Romuald Aufrere, and Frédéric Chausse. Accurate road following and reconstruction by computer vision. volume 3, pages 261 – 270. IEEE, Transactions on Intelligent Transportation Systems, 2002.

[3] Yang Cheng and Tarunraj Singh. Efficient particle filtering for road-constrained target tracking. 43, 2007.

[4] Jannik Fritsch, Tobias Kuehnl, and Andreas Geiger. A new performance measure and evaluation benchmark for road detection algorithms. In *IEEE 16th International Conference on Intelligent Transportation Systems (ITSC)*, pages 1693 – 1700, 2013.

[5] Xiao Hu, Sergio A. Rodríguez F., and Alexander Gepperth. A multi-modal system for road detection and segmentation. pages 1365 – 1370. IEEE, Intelligent Vehicles Symposium Proceedings, 2014.

[6] Zhentao Hu, Yong Jin, Jie Li, and Xianxing Liu. Maneuvering target tracking algorithm based on multiple model rao-blackwellised particle filter. *Journal of Information and Computational Science*, 8, 2012.

[7] Lim Jaechan. The joint probabilistic data association filter (jpdaf) for multi-target tracking. Technical report, Stony Brook University, 2006.

[8] Julian F. P. Kooij, Nicolas Schneider, and Dariu M. Gavrila. Analysis of pedestrian dynamics from a vehicle perspective. pages 1445 – 1450. IEEE, Intelligent Vehicles Symposium Proceedings, 2014.

[9] Emilio Maggio and Andrea Cavallaro. Learning scene context for multiple object tracking. volume 18, pages 1873 – 1884. Transactions on Image Processing, IEEE, 2009.

[10] Emilio Maggio, Elisa Piccardo, Carlo Regazzoni, and Andrea Cavallaro. Particle phd filtering for multi-target visual tracking. volume 1, pages I–1101 – I–1104. IEEE International Conference on Acoustics, Speech and Signal Processing, 2007.

[11] Umut Orguner, Thomas Schön, and Fredrik Gustafsson. Improved target tracking with road network information. pages 1 – 11, 2009.

[12] Marek Schikora, Amadou Gning, and Lyudmila Mihaylova. Box-particle phd filter for multi-target tracking. pages 106 – 113. 15th International Conference on Information Fusion (FUSION), 2012.

[13] Naoki Shibata, Seiji Sugiyama, and Takahiro Wada. Collision avoidance control with steering using velocity potential field. pages 438 – 443. IEEE, Intelligent Vehicles Symposium Proceedings, 2014.

[14] Blackman S.S. Multiple hypothesis tracking for muliple target tracking. 19:5 – 18, 2004.

[15] Sarah Strygulecy, Dennis Muller, Mirko Meuter, Christian Nunn, Sharmila (Lali) Ghosh, and Christian Wohlery. Road boundary detection and tracking using monochrome camera images. pages 864 – 870. IEEE, 16th International Conference on Information Fusion (FUSION), 2013.

[16] M. Ulmke and W. Koch. Road map extraction using gmti tracking. pages 1 – 7. IEEE, 9th International Conference on Information Fusion (FUSION), 2006.

[17] Ba-Ngu Vo and Wing-Kin Ma. The gaussian mixture probability hypothesis density filter. volume 54, pages 4091 – 4104. Transactions on Signal Processing, IEEE, 2006.

[18] Ba-Ngu Vo, Sumeetpal Singh, and Arnaud Doucet. Sequential monte carlo implementation of the phd filter for multi-target tracking. 2:792 – 799, 2003.

[19] Yunmei Zheng, Zhiguo Shi, Rongxing Lu, Shaohua Hong, and Xuemin (Sherman) Shen. An efficient data-driven particle phd filter for multi-target tracking. 9:2318 – 2326, 2013.